Journal of
Ceramic Science
and Technology

Hot Corrosion Behavior of ZrB$_2$-SiC-Graphite Composite in NaCl and Na$_2$SO$_4$ Molten Salts

X. Liu[1], G. Wang[2], L. Liu[2], Z. Wang[1], Z. Wu[1], M. Liu[*1]

[1]School of Aeronautics and Astronautics, Faculty of Vehicle Engineering and Mechanics, State Key Laboratory of Structural Analysis for Industrial Equipment, Dalian University of Technology, Dalian 116024, China.
[2]Beijing Institute of Aerospace Systems Engineering, Beijing 100076, China.

Abstract

In the present work, the hot corrosion behavior of ZrB$_2$-SiC-graphite (G) composite in different media at 900 and 1000 °C was investigated in detail. The results indicated that the ZrB$_2$-SiC-G composite became slightly corroded in NaCl molten salts owing to the ZrB$_2$ phase of the ZrB$_2$-SiC-G composite being oxidized by oxygen molecules dissolved in the NaCl molten salts. However, the ZrB$_2$-SiC-G composite underwent more severe corrosion in Na$_2$SO$_4$ molten salts, owing to the complex oxidation and sulfidation reaction of the ZrB$_2$-SiC-G composite exposed to oxygen molecules and decomposition products of Na$_2$SO$_4$ at high temperature.

Keywords: ZrB$_2$-based composites, molten salts, hot corrosion, sulfidation

I. Introduction

Zirconium diboride (ZrB$_2$) as an ultra-high temperature ceramic has attracted considerable interest owing to its extremely high melting temperatures (> 3000 °C), high hardness (22 GPa), high thermal conductivity (65 ~ 135 Wm^{-1}K^{-1}), good oxidation and ablation resistance[1-8]. In view of its good performances at extremely high temperature, ZrB$_2$ ceramic has been considered as a candidate material for use in thermal protection systems and other components of hypersonic aerospace vehicles[9-11]. Although ZrB$_2$ ceramic has many advantages, its intrinsic brittle characteristic results in poor thermal shock resistance and prevents it from being widely used, especially for applications in extreme environments[12-15]. The addition of appropriate amounts of SiC and graphite flake (G) is an effective method to improve the comprehensive performance of ZrB$_2$-based composites. SiC not only can enhance the mechanical properties, it can also improve the oxidation resistance of ZrB$_2$ by promoting the formation of silicate-based glasses that inhibit oxidation at temperatures between 800 and 1800 °C [16, 17]. The graphite flake introduced into the ZrB$_2$-SiC composite can increase fracture toughness and improve thermal shock resistance, compared with the ZrB-SiC composites[18, 19]. Therefore, ZrB$_2$-SiC-G composite is currently considered as a promising candidate for use in extreme high temperature [20, 21]. Based on these potential applications, it is necessary to investigate the corrosion behavior of ZrB$_2$-SiC-G composite in a harsh environment.

Some works have reported on the corrosion behavior of ZrB$_2$ powders and ZrB$_2$-based composites in different corrosion environments at room temperature. Lee *et al.* [22] investigated the corrosion behavior of ZrB$_2$ powders during wet processing. They found that the surfaces of both the pristine and corroded powders were predominantly covered with ZrOH, and a certain amount of Zr-B bonding. Huang *et al.* studied the corrosion behavior of ZrB$_2$ in water and concluded that a thin ZrO$_2$ layer measuring 4.67 nm was formed on the ZrB$_2$ surface after 1 h immersion in water[23]. Monticelli *et al.* studied the electrochemical corrosion behavior of ZrB$_2$ in aqueous acid solutions containing different aggressive anions (i.e. sulfates, perchlorates, chlorides, fluorides and oxalates) [24]. They found that ZrB$_2$ had converted into both insoluble (mainly ZrO$_2$) and soluble (boric acid and complexes of the different anions with Zr(IV)) corrosion products. Furthermore, the corrosion behavior of ZrB$_2$-20 vol% SiC composites during exposure to aqueous acid or neutral solutions was also studied by Monticelli *et al.* [25]. They found that the corrosion process of ZrB$_2$ was not affected by the presence of the SiC reinforcement in the composites. Lavrenko *et al.* studied the electrochemical oxidation of ZrB$_2$ and MoSi$_2$ refractory compounds as well as ZrB$_2$-MoSi$_2$ ceramics on exposure to 3 % NaCl solution[26]. The highest corrosion resistance was observed in the case of composites with a small amount (5 ~ 10 wt%) of MoSi$_2$ owing to their stable passivation at comparatively low anodic potentials. Hot corrosion is defined as accelerated corrosion that results from the presence of salt contaminants such as Na$_2$SO$_4$, NaCl and V$_2$O$_5$[27-29]. Molten salt technology has been widely applied in the industrial world because of its physical and chemical characteristics, especially its high

* Corresponding author: haerbinliuxin@163.com

electrical conductivity, high processing rate, and high diffusion rate. And recently, it has attracted a great deal of attention in the fields of jet engines, fuel cells, catalysts, and metal refinement. Unfortunately, there is lack of information regarding the hot corrosion behavior of ZrB_2-based composites in molten salt at high temperature.

In this paper, the hot corrosion behavior of ZrB_2 plus 20 vol% SiC plus 15 vol% graphite flake (ZrB_2-SiC-G) composite in different molten salt conditions (i.e. NaCl molten salts at (i) 900 °C and (ii) 1000 °C, respectively; Na_2SO_4 molten salts at (iii) 900 °C and (iv) 1000 °C, respectively) was investigated and the hot corrosion mechanism of the ZrB_2-SiC-G composite was discussed.

II. Experimental Procedure

Commercially available ZrB_2 powders (Dandong Chemical Co. Ltd., Dandong, China.) have a purity of 99.5 % and mean particle size of 2 μm. The SiC powders (Weifang Kaihua Micro-powder Co. Ltd., China.) have a purity of 99.5 % and a mean particle size of 1 μm. The graphite flakes (Qingdao Tiansheng Graphite Co. Ltd., China) with a thickness of 15 μm and mean diameter of 1 ~ 2 μm have a purity of 99 %. The mixture of ZrB_2 plus 20 vol% SiC plus 15 vol% graphite flake (ZrB_2-SiC-G) was ball-mixed for 10 h in a polyethylene bottle using ZrO_2 balls and ethanol as the grinding media. After mixing, the slurry was dried and then the mixture was hot-pressed at 1900 °C for 1 h under a uniaxial load of 30 MPa in Ar atmosphere. The specimens with dimensions of 4 mm × 6 mm × 10 mm (weighing about 1.2 g) were cut from a disk with the electrical spark cutting method. The boron carbide and diamond were mixed in water to form an abrasive paste with high solids, and the SiC sand paper was coated with the abrasive paste. Finally, specimens were ground successively employing SiC sand paper (normal 320, 400 and 600 grit) coated with the abrasive paste and then the specimens were cleaned ultrasonically in ethanol and dried at 80 °C for 1 h. NaCl (1.0 kg) and Na_2SO_4 (1.0 kg) as corrosive media were individually filled into an alumina crucible and the alumina crucible was placed in a resistance furnace (1300 °C, SX2 – 36 – 12, Suzhou Jiangdong Precise instruments Co., LTD, China). The corrosion tests were conducted in the alumina crucible in resistance furnaces in static air at 900 and 1000 °C using NaCl and Na_2SO_4 as corrosive media, respectively, for 30 min because the melting point of NaCl and Na_2SO_4 are close to 801 °C and 884 °C, respectively. The temperature at the center of the alumina crucible was monitored with a platinum-rhodium thermocouple (0 – 1400 °C, WRR, Shanghai Wolan instrument Co., LTD, China) fixed in an alumina tube. When the temperature of the salt was stabilized at the desired temperature (900 °C and 1000 °C), the dried specimen was immersed in the melting salts for 30 min, and then the specimen was taken out and cooled with dried nitrogen. For comparison, some specimens were exposed directly to static air at 1000 °C for 30 min. Since sodium chloride and sodium sulfate can be dissolved in glycerin, and other salts (sodium borate and boron sub-oxides) cannot be dissolved in glycerin, the surface of the corroded specimens is repeatedly scrubbed using glycerol (AR, Linyi Lvshen Chemical Co., Ltd. Shandong China) in order to remove the residual molten salts after hot corrosion. The phase compositions of ZrB_2-SiC-G composite after hot corrosion in different conditions were investigated with a Rigaku D/max-rb X-ray diffractometer (XRD). The morphology of the specimens after hot corrosion was investigated with a Holland FEI Sirion scanning electron microscope (SEM) equipped with an energy-dispersive spectroscopy (EDS).

III. Results and Discussion

Macrographs of specimens before and after hot corrosion tests are shown in Fig. 1. It can be seen that there are slight changes after hot corrosion in NaCl molten salts at 900 °C and 1000 °C as shown in Fig. 1(b) and (c), respectively, compared with macrograph of the specimen before the hot corrosion tests as shown in Fig. 1(a). The starting position of hot corrosion is mainly along the corners of the specimen, resulting in the corners becoming rounded, so there are strong edge effects in the test period of hot corrosion as shown in Fig. 1(b) and (c). The hot corrosion firstly spreads from the corners to the center of the specimen, and then spreads over the whole surface of specimen. A white oxide layer is formed on the surface of the specimens, which is quite similar to the result of isothermal oxidation tests in air at 1000 °C, as shown in Fig. 1(f) which indicates that the ZrB_2-SiC-G composite undergoes a slight corrosion attack owing to the strong corrosion resistance of ZrB_2, SiC and graphite to NaCl molten salts. Fig. 1(d) shows the clear evidence of corrosion attack on the surface of the specimen with a loose oxide layer corroded in Na_2SO_4 molten salts at 900 °C for 30 min. As the temperature increased up to 1000 °C, the macro-morphology of the surface of the specimen shows obvious change as shown in Fig. 1(e). In addition, the poor adhesion between the oxide layer and substrates results in peeling phenomena of the oxide layer. Compared with the specimen corroded in NaCl molten salts, the ZrB_2-SiC-G composite underwent more severe corrosion in Na_2SO_4 molten salts.

(1) Composition analysis

Fig. 2 shows the XRD pattern of the surface of the scrubbed specimen after hot corrosion in NaCl molten salts at different temperatures and the XRD pattern of isothermal oxidation in static air is used for comparison. It is evident that the compositions of the surface are mainly composed of a small amount of ZrO_2, $NaBO_2$ and $Na_{10}B_4O_{11}$, which indicates that the ZrB_2-SiC-G composite undergoes obvious corrosion. During the isothermal oxidation in static air, the graphite flake is firstly oxidized to CO and/or CO_2 at above 500 °C. When the temperature rises to 900 °C, the boron element reacts with oxygen to generate a protective B_2O_3 layer on the surface of the ZrB_2-SiC-G composite, meanwhile, the zirconium element reacts with oxygen to generate ZrO_2[30, 31]. Because the oxidation rate of SiC is much slower than that of ZrB_2 in this temperature regime (≤1000 °C), the SiC particles do not oxidize appreciably[32, 33]. Earlier studies have also concluded that B_2O_3 is an effective barrier to the transport of oxygen, which can reduce the corrosion rate in static air[34, 35]. However, the escape of CO and/or CO_2 promotes the volatilization of B_2O_3 layer.
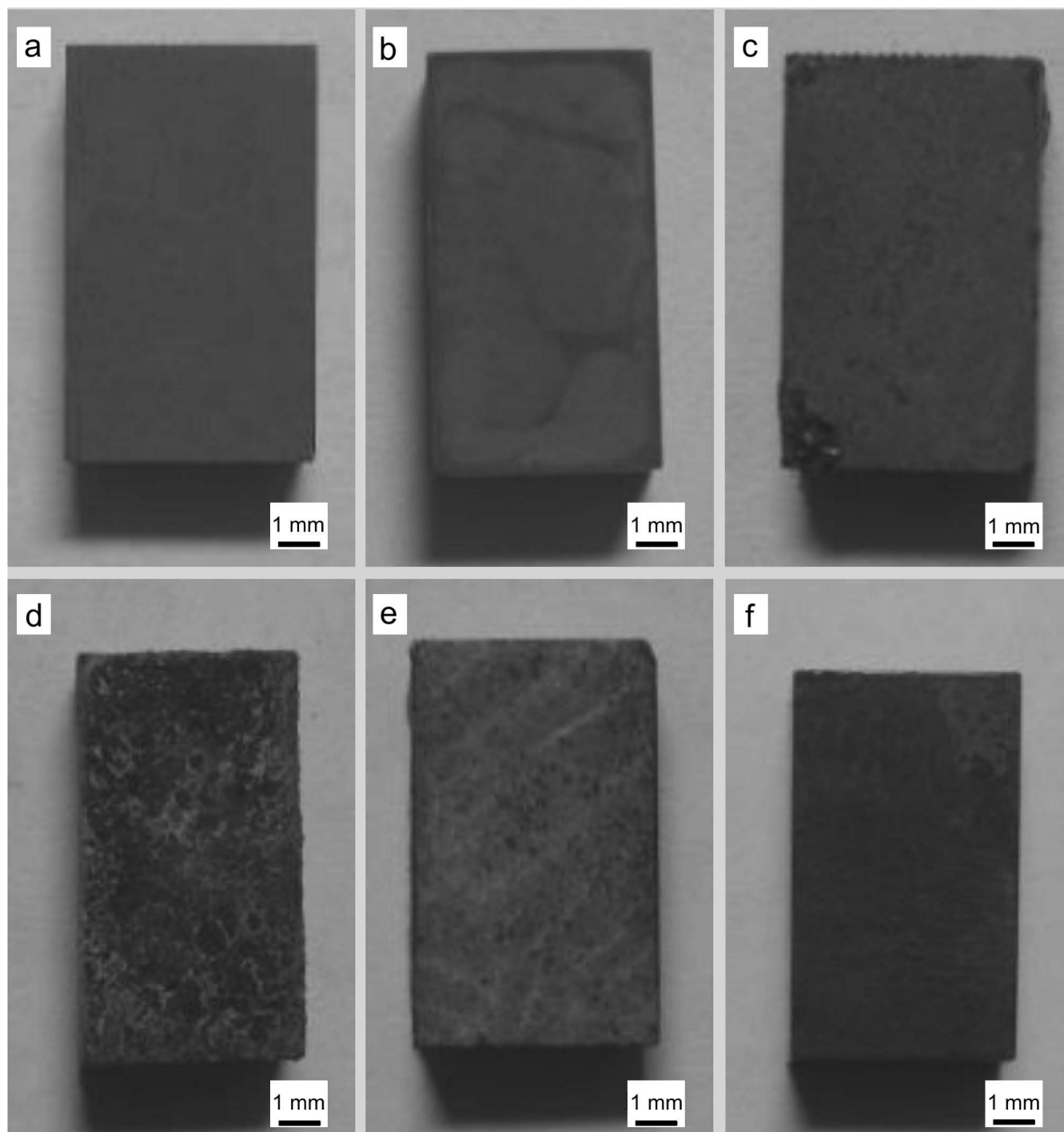
Fig. 1: Macrographs of specimens after hot corrosion test for 30 min; (a) before test; (b) hot corrosion in NaCl molten salts at 900 °C; (c) hot corrosion in NaCl molten salts at 1000 °C; (d) hot corrosion in Na$_2$SO$_4$ molten salts at 900 °C; (e) hot corrosion in Na$_2$SO$_4$ molten salts at 1000 °C; (f) oxidation in static air at 1000 °C.

The ZrO$_2$ peak intensity represents the corrosion rate, so the corrosion rate for different corrosion conditions has been found to increase in the following order: in NaCl molten salts at 900 °C < in NaCl molten salts at 1000 °C < in static air at 1000 °C. This result is due to the inertia of NaCl to the specimen and a good fluidity of NaCl. The corrosion behavior is mainly attributed to the specimen reacting with oxygen molecules dissolved in the NaCl molten salts. The whole specimen was immersed in NaCl molten salts with good fluidity during the test process. Therefore, the dissolution and diffusion of oxygen

molecules in NaCl molten salts are limited. When the oxygen molecules were reduced, the specimen is protected by NaCl molten salts from oxidation by obstructing the rapid contact between specimen and oxygen molecules. Furthermore, it is expected that the amorphous phases including B$_2$O$_3$ and SiO$_2$ are formed. Therefore, a borosilicate is not detected by X-ray diffractometer because the content of a borosilicate is too low for the detection limit (approximately 5 %) of the X-ray diffractometer owing to the high vapor pressure of the B$_2$O$_3$ and low oxidation rate of the SiC phase.
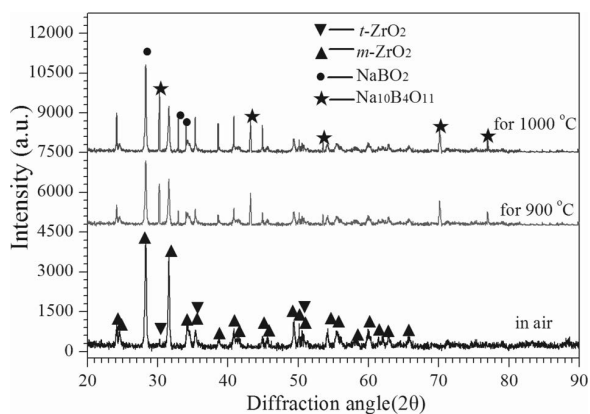
Fig. 2: XRD patterns of specimen surfaces after oxidation in static air and hot corrosion in NaCl molten salts for 30 min.

The XRD patterns of the surface of the specimen were also obtained to investigate the corrosion products in Na_2SO_4 molten salts at 900 and 1000 °C for 30 min as shown in Fig. 3. Compared with corrosion of the ZrB_2-SiC-G composite in NaCl molten salts and static air, a great change in the composition is detected for the specimen corroded in Na_2SO_4 molten salts. The sharpening of the characteristic peaks of ZrO_2 and $NaBO_2$ is noticeable. As shown in Fig. 3, the corrosion temperature does not affect the corrosion products but the corrosion rate. There is an obvious difference between the XRD patterns of the two specimens corroded at different temperature; namely, the characteristic peaks in the XRD patterns of the product obtained at 900 °C were significantly lower than that at 1000 °C. The sodium oxysulfides are readily

detected, and other complex compounds may also exist, however, have not been detected owing to their low content. The ZrO_2 peak intensity is qualitatively used again to characterize the corrosion rate, so the corrosion rate for different corrosion conditions has been found to increase in the following order: in static air at 1000 °C < in Na_2SO_4 molten salts at 900 °C < in Na_2SO_4 molten salts at 1000 °C. This result is due to a loose oxide layer, activity of Na_2SO_4 and the peeling phenomena of the oxide layer, which will be discussed later.

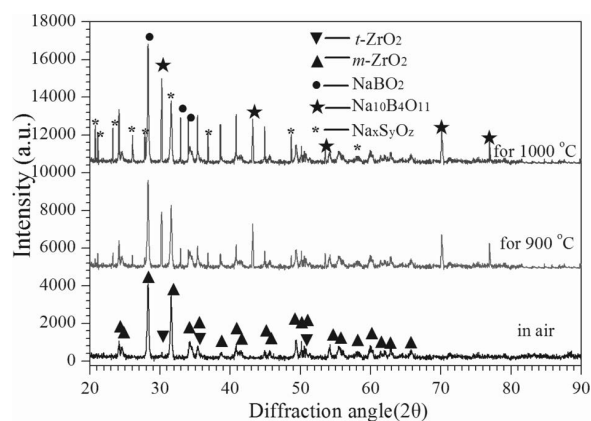**Fig. 3:** XRD patterns of specimen surfaces after oxidation in static air and hot corrosion in Na_2SO_4 molten salts for 30 min.

(2) Microstructure

The micrographs of the surface of the specimen after hot corrosion in NaCl molten salts at 900 and 1000 °C are shown in Fig. 4.
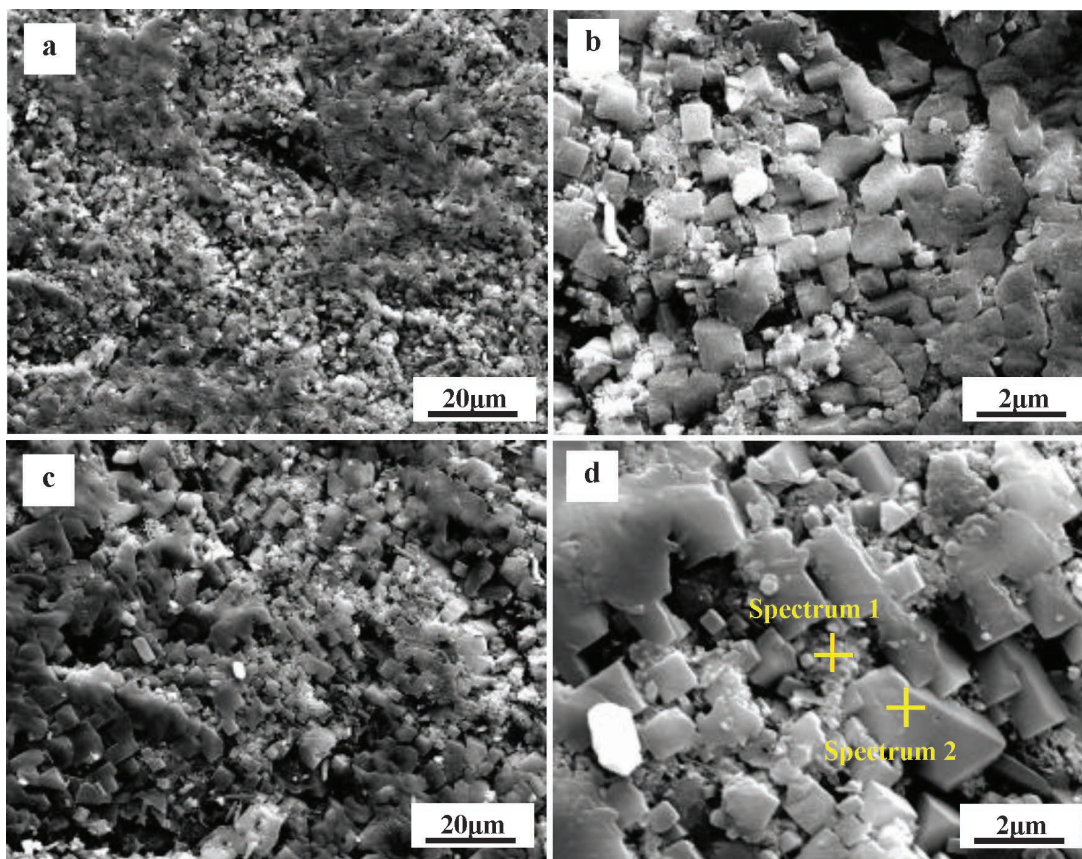

Fig. 4: SEM images of surface of specimen after hot corrosion tests in NaCl molten salts at 900 ° C and 1000 °C for 30 min: (a) and (b) for 900 °C; (c) and (d) for 1000 °C; (a) and (c) is low magnification; (b) and (d) is high magnification.

It can be seen that the surface of the specimen has become rough and is covered with cuboid-like grains with an average size of about 1 μm (hot corrosion at 900 °C) and 2 μm (hot corrosion at 1000 °C). EDS was used to test the composition of the oxide layer. However, the results (listed in Table 1) of the EDS analysis for positions 1 and 2 are qualitative owing to its low sensitivity to light elements (i.e. boron)[35]. The results of EDS (Table 1) and XRD (Fig. 2) indicate that formed grains are mainly composed of ZrO_2 covered with a trace borosilicate glass layer. The borosilicate glass forms because the oxidation of SiC is much slower than that of ZrB_2 at 900 or 1000 °C and the trace SiO_2 can react with B_2O_3 to generate borosilicate glass [33]. The borosilicate glass layer is a kind of compound glass consisting of SiO_2, B_2O_3, $NaBO_2$ and ZrO_2. The ZrO_2 grain size becomes larger as the hot corrosion temperature increases to 1000 °C in NaCl molten salts. A large number of pits are found on the surface of the specimen after hot corrosion owing to the escape of gaseous products, such as CO and/or B_2O_3.

SEM images of the surface of the specimen after hot corrosion in Na_2SO_4 molten salts at 900 °C are shown in Fig. 5. As shown in Fig. 5(a) and (b), an oxide layer with coarser particles is formed on the surface of the specimen. The EDS results obtained from Spectrum 3 in Fig. 5(a) and Spectrum 4 in Fig. 5(b) demonstrate that the particles are mainly composed of O, Na, Si, Zr and S, and the oxide layer is mainly composed of O, Na, Si, Zr, as listed in Table 1. Although the boron element does exist, the sensitivity of EDS to light elements (i.e. boron) is too low to detect the boron element [35]. In combination with the XRD analysis (in Fig. 3), it could be found that the particles are mainly composed of ZrO_2, $NaBO_2$, $Na_{10}B_4O_{11}$ and $Na_xS_yO_z$.

The formation of the oxide layer with multiple-phase particles is due to following reactions: (i) ZrB_2 and SiC react with oxygen molecules dissolved in Na_2SO_4 molten salts; (ii) ZrB_2 and SiC react with Na_2SO_4 molten salts at high temperature. Because the oxide layer can obstruct the contact between the specimen and Na_2SO_4 molten salts, which, to some extent, prevents the specimen from further reacting with Na_2SO_4 molten salts. So the corrosion rate of the specimen corroded in Na_2SO_4 molten salts at 900 °C was slightly higher than that of the specimen oxidized in static air at 1000 °C. The micrographs of the specimen surface after hot corrosion in Na_2SO_4 molten salts at 1000 °C are shown in Fig. 5(c) and (d). Obviously, hot corrosion of specimen in Na_2SO_4 molten salts at 1000 °C is more severe than that at 900 °C, which results in the formation of porous and loose structures on the surface of the specimen. As shown in Fig. 5(c) and (a), the discontinuous layer with the loose products covering the surface after hot corrosion at 1000 °C is different from that after hot corrosion at 900 °C. Although the surface of the oxide layer is coated with a glass layer as shown in Table 1 Spectrum 5, the poor adhesion between the oxide layer and the substrate results in the peeling of the oxide layer. So the oxide layer with glass layer could not inhibit a severe corrosion attack on the surface of the specimen. The corrosion rate for the specimen corroded in Na_2SO_4 molten salts at 1000 °C was obviously greater than that of the specimen for hot corrosion at 900 °C.
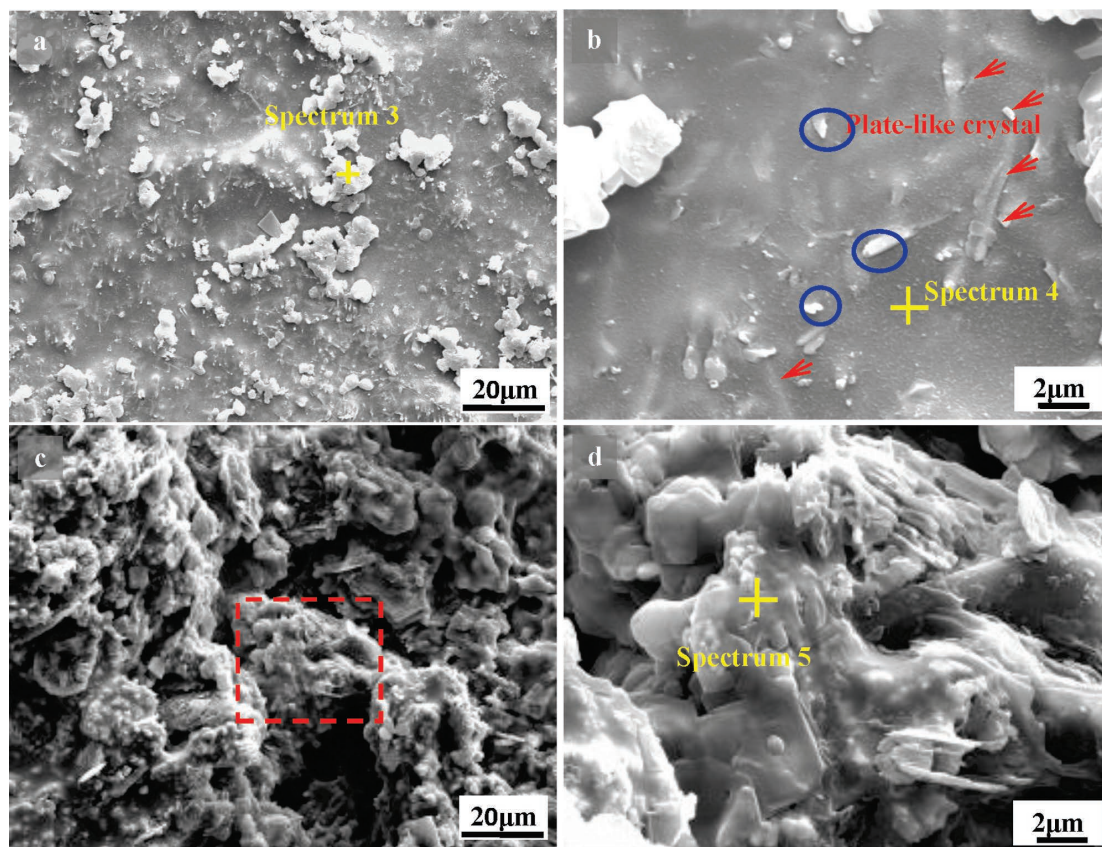
Fig. 5: SEM images of surfaces of specimen after hot corrosion tests in Na_2SO_4 molten salts at 900 °C and 1000 °C for 30 min: (a) and (b) for 900 °C; (c) and (d) for 1000 °C; (a) and (c) is low magnification; (b) and (d) is high magnification.

Table 1: Element content of EDS analysis for different positions.

Positions	Elements (wt%)					
	Zr	B	Si	O	Na	S
1	21.2	0.2	16.3	55.2	7.1	0.0
2	28.2	0.3	15.9	49.5	6.1	0.0
3	21.6	0.1	16.5	45.6	6.7	9.5
4	18.6	0.5	18.5	46.3	5.5	10.6
5	15.9	0.4	19.6	47.6	6.6	9.9

SEM images of cross-sections of specimens corroded in NaCl molten salts at 900 and 1000 °C are shown in Fig. 6(a) and (b), respectively. There are no obvious differences between the two morphologies of specimens, implying that the specimens experience a similar corrosion process in NaCl molten salts at 900 and 1000 °C. The thin oxide layer is readily detected and the obvious interface between the oxide layer and substrates is not detected, which indicates that ZrB_2 has good resistance to NaCl molten salts at high temperature. The cross-section images of the specimen after corrosion in Na_2SO_4 molten salts at 900 and 1000 °C are presented in Fig. 6(c) and (d),

respectively. The oxide layer on the surface of specimens is readily observed in the cross-section images, which is because the oxide layer is loose and there is poor adhesion between the oxide layer and the substrate, which results in the peeling phenomena of oxidation layer. The rough strippable layer with the thickness of 20 μm was formed on the surface of the specimen corroded in Na_2SO_4 molten salts at 1000 °C. Furthermore, open pores existed not only in the layer and interlayer, but also between the substrate and the oxide layer. The porous and loose layer loses its protective properties and acts as channels for oxygen and molten salts diffusing into the substrates.
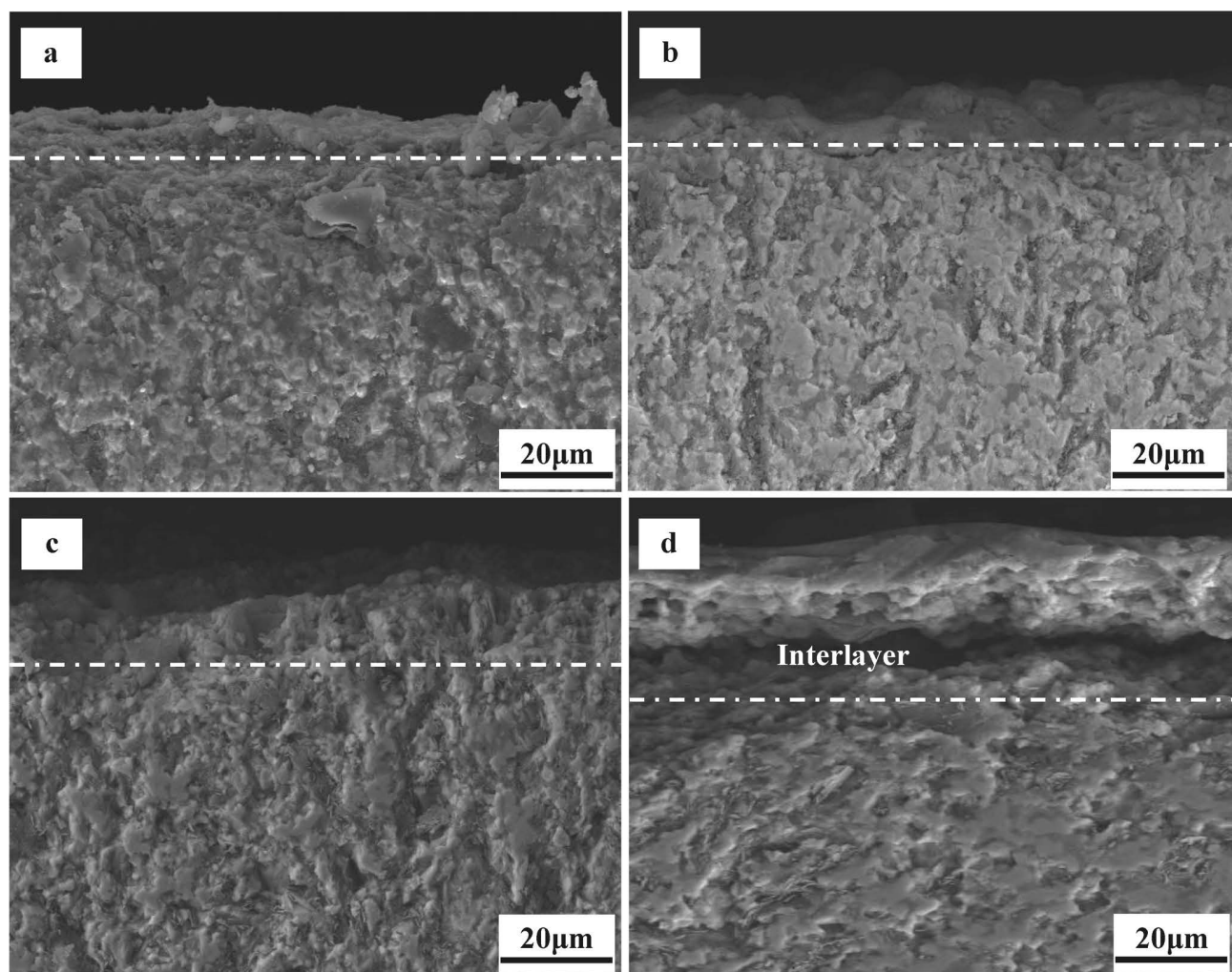

Fig. 6: Cross-section morphology of specimens after hot corrosion test for 30 min: hot corrosion in NaCl molten salts at 900 °C (a) and 1000 °C (b); hot corrosion in Na_2SO_4 molten salts at 900 °C (c) and 1000 °C (d).

The internal oxidation and sulfidation occurred when the Na$_2$SO$_4$ molten salts quickly diffused into the substrate through the pores. The hot corrosion was along the oxide layer and grain boundary and a large interlayer between substrate and layer was formed, which promoted the corrosion of the specimen. The structural features result in different corrosion rates for different corrosion conditions: in static air at 1000 °C < in Na$_2$SO$_4$ molten salts at 900 °C < in Na$_2$SO$_4$ molten salts at 1000 °C.
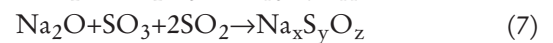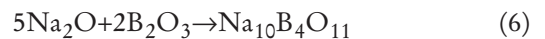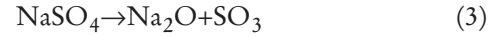
(3) Hot corrosion mechanism

Based on the above experimental observations and analysis, the hot corrosion mechanism of the ZrB$_2$-SiC-G composite in molten salts can be summarized as follows and the schematic illustration of the hot corrosion process of the ZrB$_2$-SiC-G composite is shown in Fig. 7.

During the hot corrosion of ZrB$_2$ phase, the ZrB$_2$ phase reacts with oxygen molecules to generate an oxide layer on the surface of the ZrB$_2$ phase in the initial corrosion stage. NaCl molten salts cannot destroy the oxide layer and diffuse into the substrate to attack the ZrB$_2$ phase. However, for the ZrB$_2$-SiC-G composite, the oxidation products such as B$_2$O$_3$, SiO$_2$ and ZrO$_2$ are formed on the surface of specimen according to Reactions (1) and (2) [36–38]. Although the NaCl molten salts and oxidation products do not react, the reaction between the specimen and oxygen molecules dissolved in NaCl molten salts is promoted at the high temperature. Then the reaction is prevented by NaCl molten salts when the oxygen molecules are reduced.

$$2ZrB_2 + 5O_2 \rightarrow 2ZrO_2 + 2B_2O_3 \qquad (1)$$
$$2SiC + 3O_2 \rightarrow 2SiO_2 + 2CO \qquad (2)$$
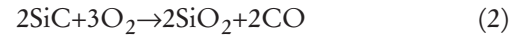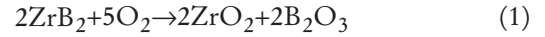
However, the hot corrosion behavior of ZrB$_2$-SiC-G composite in Na$_2$SO$_4$ molten salts is different from that in NaCl molten salts. In the interface between the Na$_2$SO$_4$ molten salts and the specimen, the Na$_2$SO$_4$ is decomposed to acidic SO$_3$ and alkaline Na$_2$O in high-temperature conditions according to Reaction (3). The SO$_3$ is decomposed to SO$_2$ and oxygen molecules according to Reaction (4) [39, 40].

$$NaSO_4 \rightarrow Na_2O + SO_3 \qquad (3)$$
$$2SO_3 \rightarrow 2SO_2 + O_2 \qquad (4)$$
$$Na_2O + B_2O_3 \rightarrow 2NaBO_2 \qquad (5)$$
$$5Na_2O + 2B_2O_3 \rightarrow Na_{10}B_4O_{11} \qquad (6)$$
$$Na_2O + SO_3 + 2SO_2 \rightarrow Na_xS_yO_z \qquad (7)$$

In Na$_2$SO$_4$ molten salts, the ZrB$_2$, SiC and C (graphite) react with oxygen molecules, some of which are from dissolution in Na$_2$SO$_4$ molten salts and others are from decomposition of Na$_2$SO$_4$. According to Reactions (1) and (2), B$_2$O$_3$, SiO$_2$ and ZrO$_2$ are produced, which results in the decrease of oxygen pressure and increase of sulfur oxide pressure in the interface between the oxide and molten salts. Sulfur oxide and oxygen are diffused into substrate through the loose oxide layer and react with substrate by internal oxidation and sulfidation. The oxidation products (mainly composed of B$_2$O$_3$, SiO$_2$ and ZrO$_2$) react with Na$_2$O to form borosilicate, NaBO$_2$ (Reaction (5)),
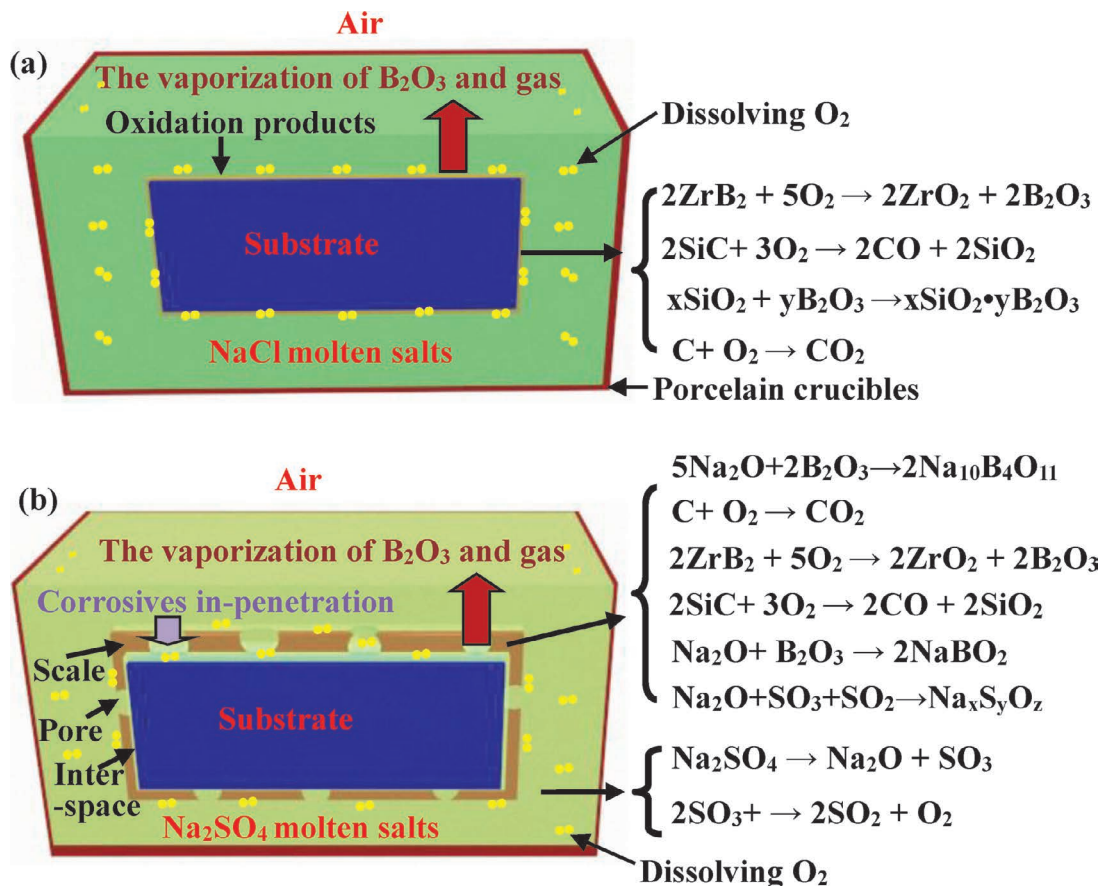

Fig. 7: Schematic illustration of the hot corrosion process of ZrB$_2$-SiC-G composites: (a) in NaCl molten salts; (b) in Na$_2$SO$_4$ molten salts.

$Na_{10}B_4O_{11}$ (Reaction (6)) and other salts containing sodium ions ($Na_xS_yO_z$(7)). The escape of CO and/or CO_2 promotes the volatilization of the B_2O_3 layer, which results in the formation of the loose pores and interlayers at higher temperature (1000 °C). The oxygen molecules and Na_2SO_4 molten salts penetrate into the substrate through the pores and destroy the continuous oxide layer, which results in the oxide layer losing its protective properties. Therefore, the hot corrosion of ZrB_2-SiC-G composite in Na_2SO_4 molten salts is more severe.

IV. Conclusions

The hot corrosion behavior of ZrB_2-SiC-G composite in different media (i.e. NaCl molten salts at 900 and 1000 °C, Na_2SO_4 molten salts at 900 and 1000 °C) was investigated. The results indicate that the ZrB_2-SiC-G composite undergoes a slight corrosion in NaCl molten salts owing to the inertia of NaCl to the specimen and a good fluidity of NaCl. The ZrB_2 phase reacts with oxygen molecules to form an oxide layer, which prevents the specimen from contacting the reducing oxygen molecules. However, the ZrB_2-SiC-G composite undergoes more severe corrosion attack in Na_2SO_4 molten salts, which is due to the complex oxidation and sulfidation reaction between original compositions of the ZrB_2-SiC-G composite, oxygen molecules and decomposition products of Na_2SO_4 at high temperature. An oxide layer composed of SiO_2, B_2O_3, $NaBO_2$, $Na_{10}B_4O_{11}$, $Na_xS_yO_z$ and ZrO_2 is formed on the surface of the ZrB_2-SiC-G composite after hot corrosion in Na_2SO_4 molten salts at 900 °C and 1000 °C. Although the oxide layer can obstruct the contact between the specimen and Na_2SO_4 molten salts and prevent the specimen from further corrosion, Na_2SO_4 still can participate in oxidation reactions of ZrB_2 and SiC phases. The loose oxide layer, activity of Na_2SO_4 and the peeling phenomenon of oxide layer result in different corrosion rates for different corrosion conditions: in static air at 1000 °C< in Na_2SO_4 molten salts at 900 °C < in Na_2SO_4 molten salts at 1000 °C.

Acknowledgments

References

1   Lin, J., Zhang, X.H., Han, J.C., Han, W.B., Zhao, W.G.: Oxidation behavior and phase transition of ZrB_2-SiC_w-ZrO_{2f} ceramic, *Corros. Sci.*, **78**, 13–21, (2014).

2   Lin, J., Huang, Y., Zhang, H., *et al.*: Characterization of hot-pressed short ZrO_2 fiber toughened ZrB_2-based ultra-high temperature ceramics, *Mater. Charact.*, **95**, 272–77, (2014).

3   Wang, L.L., Fang, G.D., Liang, J., Wang, C.: Formation mechanism and high temperature mechanical property characterization of SiC depletion layer in ZrB_2/SiC ceramics, *Mater. Charact.*, **95**, 245–51, (2014).

4   Asl, M.S., Nayebi, B., Ahmadi, Z., *et al.*: Fractographical characterization of hot pressed and pressureless sintered SiAlON-doped ZrB_2-SiC composites, *Mater Charact.*, **102**, 137–45, (2015).

5   Raua, J.V., Ferrob, D., Falconec, M.B., Generosia, A., Rossi Albertinia, V., *et al.*: Hardness of zirconium diboride films deposited on titanium substrates, *Mater. Chem. Phys.*, **112**, 504–09, (2008).

6   Tian, W.B., Kann, Y.M., Zhang, G.J., Wang, P.L.: Effect of carbon nanotubes on the properties of ZrB_2-SiC ceramics, *Mater. Sci. Eng. A.*, **487**, 568–73, (2008).

7   Zimmermann, J.W., Hilmas, G.E., Fahrenholtz, W.G.: Thermophysical properties of ZrB_2 and ZrB_2-SiC ceramics, *J. Am. Ceram.Soc.*, **91**, 1405–11, (2008).

8   Guo, S.Q., Kagawa, Y., Nishimura, T., Tanaka, H.: Thermal and electrical properties in hot-pressed ZrB_2-$MoSi_2$-SiC composites, *J. Am. Ceram. Soc.*, **90**, 2255–58, (2007).

9   Fahrenholtz, W.G.: Thermodynamic analysis of ZrB_2-SiC Oxidation: formation of a SiC-depleted region, *J. Am. Ceram. Soc.*, **90**, [1], 143–48, (2007).

10   Opeka, M.M., Talmy, I.G., Zaykoski, J.A.: Oxidation-based materials selection for 2000 °C + hypersonic aerosurfaces: theoretical considerations and historical experience, *J. Mater. Sci.*, **39**, 5887–904, (2004).

11   Van Wie, D.M., Drewry Jr, D.G., King, D.E., Hudson, C.M.: The hypersonic environment: required operating conditions and design challenges, *J. Mater. Sci.*, **39**, 5915–24, (2004).

12   Zhang, X.H., Xu, L., Du, S.Y., Han, J.C., Hu, P., *et al.*: Fabrication and mechanical properties of ZrB_2-SiC_w ceramic matrix composite, *Mater. Lett.*, **62**, 1058–60, (2008).

13   Yang, F.Y., Zhang, X.H., Han, J.C., Du, S.Y.: Processing and mechanical properties of short carbon fibers toughened zirconium diboride-based ceramics, *Mater. Des.*, **29**, 1817–20, (2008).

14   Wang, Y.G., Liu, W., Cheng, L.F., Zhang, L.T.: Preparation and properties of 2D C/ZrB_2-SiC ultra high temperature ceramic composites, *Mater. Sci. Eng. A.*, **524**, 129–33, (2009).

15   Yang, F.Y., Zhang, X.H., Han, J.C., Du, S.Y.: Characterization of hot-pressed short carbon fiber reinforced ZrB_2-SiC ultra-high temperature ceramic composites, *J. Alloy. Compd.*, **472**, 395–99, (2009).

16   Han, J.C., Hu, P., Zhang, X.H., Meng, S.H.: Oxidation behaviour of zirconium diboride-silicon carbide at 1800 °C, *Scripta Mater.*, **57**, 825–2, (2007)

17   Vijay, V., Bhuvaneswari, S., Biju, V.M.: Influence of titanium silicide active filler on the microstructure evolution of borosiloxane-derived Si-B-O-C ceramics, *J. Ceram. Sci. Technol.*, **7**, [1], 97–105, (2016).

18   Zhang, X.H., Wang, Z., Sun, X., Han, W.B., Hong, C.Q.: Effect of graphite flake on the mechanical properties of hot pressed ZrB_2-SiC ceramics, *Mater. Lett.*, **62**, 4360–62, (2008).

19   Wang, Z., Hong, C.Q., Zhang, X.H., Sun, X., Han, J.C.: Microstructure and thermal shock behavior of ZrB_2-SiC-graphite composite, *Mater. Chem. Phys.*, **113**, 338–41, (2009)

20   Chen, H.B., Wang, Z., Meng, S.H., Bai, G.H., Qu, W.: The failure mechanism of ZrB_2-SiC-graphite composite heated by high electric current, *Mater. Lett.*, **63**, 2346–48, (2009).

21   Zhang, X.H., Wang, Z., Hu, P., Han, W.B., Hong, C.Q.: Mechanical properties and thermal shock resistance of ZrB_2-SiC ceramic toughened with graphite flake and SiC whiskers, *Scripta Mater.*, **61**, 809–12, (2009).

22   Lee, S.H., Sakka, Y., Kagawa, Y.: Corrosion of ZrB_2 powder during wet processing-analysis and control, *J. Am. Ceram. Soc.*, **91**, 1715–17, (2008).

23   Huang, T., Hilmas, G.E., Fahrenholtz, W.G., Leu, M.C.: Dispersion of zirconium diboride in an aqueous, high-solids paste, *Int. J. Appl. Ceram. Technol.*, **4**, 470–79, (2007).

24   Monticelli, C., Bellosi, A., Dal Colle, M.: Electrochemical behavior of ZrB_2 in aqueous solutions, *J. Electrochem. Soc.*, **151**, B331–B339, (2004).

25   Monticelli, C., Zucchi, F., Pagnoni, A., Dal Colle, M.: Corrosion of a zirconium diboride/silicon carbide composite in aqueous solutions, *Electrochim. Acta*, **50**, 3461–69, (2005).

26 Lavrenko, V.O., Shvets, V.A., Talash, V.M., Kotenko, V.A., Khomko, T.V.: Electrochemical oxidation of ZrB₂-MoSi₂ ceramics in a 3 % NaCl solution, *Powder Metall. Met. Ceram.*, **50**, 749 – 53, (2012).

27 Zhao, G., Huang, C., He, N.: Mechanical properties, strengthening and toughening mechanisms of reactive-hot-pressed TiB₂-SiC-Ni ceramic composites, *J. Ceram. Sci. Technol.*, **8**, [2], 233 – 242, (2017).

28 Uusitalo, M.A., Vuoristo, P.M.J., Mäntylä, T.A.: High temperature corrosion of coatings and boiler steels below chlorine-containing salt deposits, *Corros. Sci.*, **46**, 1311 – 31, (2004).

29 Wang, L., Cheng, J., Qiao, Z.: Tribological behaviors of in situ TiB₂ ceramic reinforced TiAl-based composites under sea water environment, *Ceram. Int.*, **43**, [5], 4314 – 4323, (2017).

30 Kazemzadeh Dehdashti, M., Fahrenholtz, W.G., Hilmas, G.E.: Effects of transition metals on the oxidation behavior of ZrB₂ ceramics, *Corros. Sci.*, **91**, 224 – 31, (2015).

31 Li, N., Hu, P., Zhang, X.H., Liu, Y.Z., Han, W.B.: Effects of oxygen partial pressure and atomic oxygen on the microstructure of oxide scale of ZrB₂-SiC composites at 1500 °C, *Corros. Sci.*, **73**, 44 – 53, (2013).

32 Smith, G., Burstein, G.T.: Degradation of the Pt/C air cathode in acidic solution examined by cyclic thermammetry, *J. Power Sources,* **196**, 9188 – 94, (2011).

33 Tripp, W.C., Graham, H.C.: Thermogravimetric study of the oxidation of ZrB₂ in the temperature range of 800 – 1500 °C, *J. Electrochem. Soc.*, **118**, 1195 – 209, (1971).

34 Burstein, G.T., Carboneras, M., Daymond, B.T.: The temperature dependence of passivity breakdown on a titanium alloy determined by cyclic noise thermammetry, *Electrochim. Acta,* **55**, 7860 – 66, (2010).

35 Kuriakose, A.K., Margrave, J.L.: The oxidation kinetics of zirconium diboride and zirconium carbide at high temperatures, *J. Electrochem. Soc.*, **111**, 827 – 31, (1964).

36 Hu, P., Wang, G.L., Wang, Z.: Oxidation mechanism and resistance of ZrB₂-SiC composites, *Corros. Sci.*, **51**, 2724 – 32, (2009)

37 Yao, X.Y., Li, H.J., Zhang, Y.L., Ren, J.J., Yao D.J., *et al.*: A SiC/ZrB₂-SiC/SiC oxidation resistance multilayer coating for carbon/carbon composites, *Corros. Sci.*, **57**, 148 – 53, (2012).

38 Tang, S.F., Deng, J.Y., Wang, S.J., Liu, W.C.: Comparison of thermal and ablation behaviors of C/SiC composites and C/ZrB₂-SiC composites, *Corros. Sci.*, **51**, 54 – 61, (2009).

39 Zhang, K., Liu, M.M., Liu, S.L., Sun, C., Wang, F.H.: Hot corrosion behaviour of a cobalt-base super-alloy K40S with and without NiCrAlYSi coating, *Corros. Sci.*, **53**, 1990 – 98, (2011).

40 Zhang, Z.T., Sridhar, S., Cho, J.W.: An Investigation of the Evaporation of B₂O₃ and Na₂O in F-Free Mold Slags. *ISIJ int.*, **51**, 80 – 87, (2011).